Journal of Seismology **7:** 65–78, 2003.

Stress fields in the Iberian-Maghrebi region

J. Henares[1], C. López Casado[1], C. Sanz de Galdeano[2], J. Delgado[3,*] & J.A. Peláez[4]
[1]*Dpto. Física Teórica y del Cosmos, Facultad de Ciencias, Universidad de Granada, 18071 Granada, Spain, e-mail: clcasado@ugr.es;* [2]*Instituto Andaluz de Ciencias de la Tierra (CSIC-Univ. Granada), Facultad de Ciencias, 18071, Granada, Spain, e-mail: csanz@ugr.es;* [3]*Author for correspondence: Dpto. Ciencias de la Tierra, Universidad de Alicante, Ap. Correos 99, 03080 Alicante, Spain, tel: +34 965 903 400, ext. 3341, fax: +34 965 903 552, e-mail: jose.delgado@ua.es;* [4]*Dpto. Física, Escuela Politécnica Superior, Universidad de Jaén, 23071 Jaén, Spain, e-mail: japelaez@ujaen.es*

Received 15 December 2000; accepted in revised form 20 March 2002

Key words: Betic Cordillera, Iberian-Maghrebi region, focal mechanism, present-day stress field

Abstract

This study concerns the present stress field between the Eurasian and African plates in the Iberian-Maghrebi region (Portugal, Spain, Morocco, Algeria and Tunisia). In addition to an up-to-date catalogue of earthquakes in this area, a catalogue of the focal mechanisms composed of 486 solutions of fault planes, standardized in terms of notation and information type, was used. These data were used applying the right-dihedron method of Angelier and Mechler (1977), to obtain different zones with homogeneous stress. The results obtained for shallow earthquakes ($h < 30$ km) coincide, in the majority of cases, with the general stress fields proposed by numerous authors for this region, according to which there is NW-SE compression. However, the stress orientation appears to vary in certain areas, perhaps perturbed by the opening of the Atlantic Ocean, the approach of Iberia and Africa, or the extension of the Alboran Sea. For the intermediate earthquakes ($30 < h < 150$ km) no general pattern was found, and the P and T axes seem to be randomly oriented for the depth intervals considered. For the very deep earthquakes ($h > 600$ km), however, the P axis lies in a NNW-SSE direction, dipping towards the SSE, while the T axis is subhorizontal in a NE-SW direction. The determinations from the focal mechanisms highlight the existence of a regional stress field with a subhorizontal compression axis trending NW-SE. Superimposed are others that specifically affect particular sectors; these are related to the opening of the Atlantic Ocean, the extension of the Betic Cordillera and the Alboran Sea, and even the present compression between the Iberian and European plates.

Introduction

The seismotectonic complexity of the Iberian-Maghrebi area is remarkable, due to the fact that the area corresponds to part of the contact between the plates of Eurasia (in particular, the Iberian subplate) and Africa. Disperse, shallow ($h < 30$ km), intermediate ($30 < h < 150$ km) and even very deep ($h > 600$ km) seismicity exists. Along the Azores to Gorringe Heights the contact between the Eurasian and African plates is clear and linear (Udías and Buforn, 1991; Figure 1), and all the earthquake foci are shallow. The same occurs in the north of Algeria and Tunisia (Udías and Buforn, 1991). However, in the zone of the Gulf of Cadiz, northern Morocco and the Alboran Sea the contact becomes more complex and the seismicity is more diffuse. Several hypotheses have been put forward to explain what is happening in this area: *intumescence and convection of the mantle* (Van Bemmelen, 1969, 1972a,b, 1973; Vissers et al., 1995), *westward movement of the internal Betic-Rif zone* (Andrieux et al., 1971; Andrieux and Mattauer, 1973; Sanz de Galdeano, 1983, 1990, 1996, 1997), *existence of subducted lithospheric laminae* (Araña and Vegas, 1974), *lithospheric delamination* (Seber et al., 1996a,b; Buforn et al., 1997; Mezcua and Rueda, 1997; Morales et al., 1997; Calvert et al., 2000) and

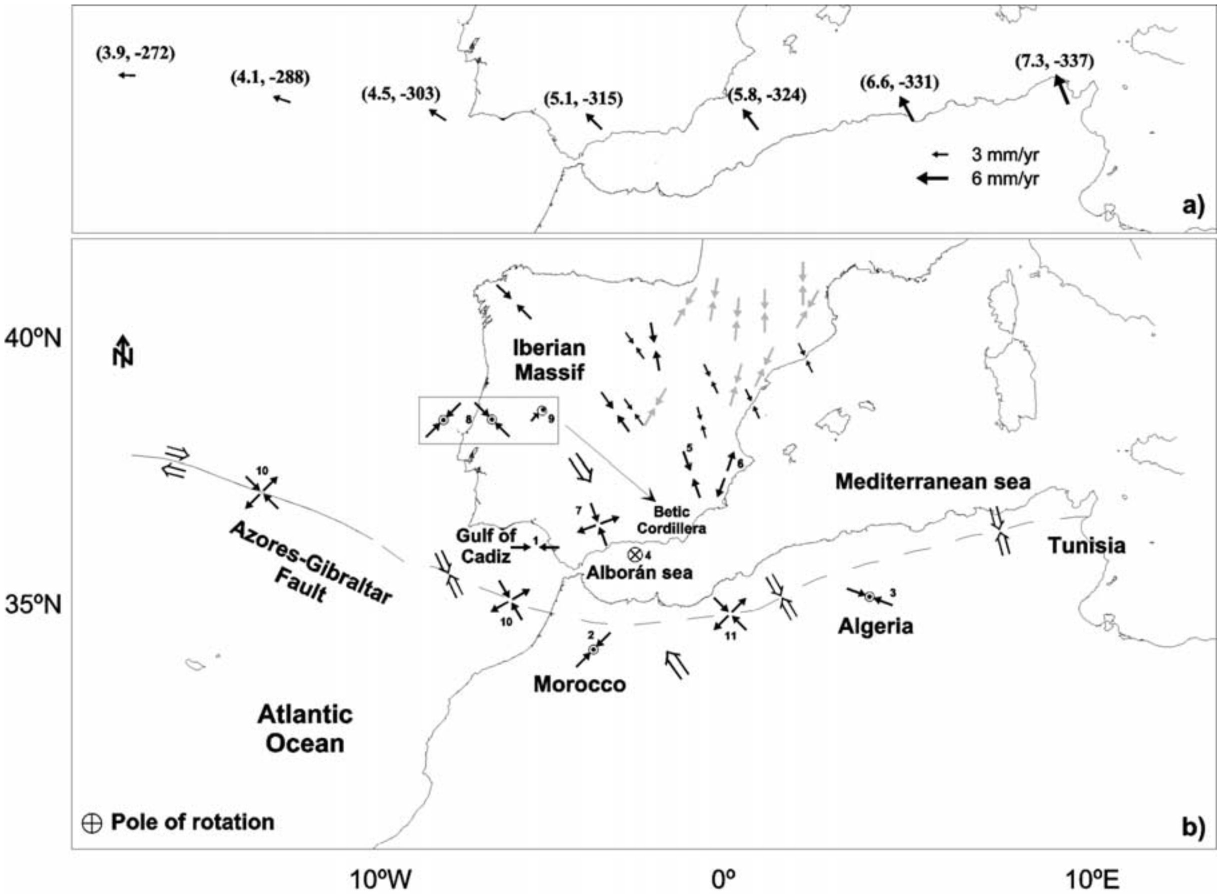

Figure 1. a) Displacement vectors according to the NUVEL-1 model (DeMets et al., 1990, 1994). The modulus and strike of the velocity vector for several chosen points are given in parentheses. b) Stress fields proposed for different areas of the Iberian-Maghrebi region, based on data from various authors. 1.– Stress field for the Azores-Gibraltar area according to Herraiz et al. (2000); 2, 3 and 4.– Stress fields for Morocco, Algeria and Alboran Sea, respectively, according to Galindo et al. (1993); 5 and 6.– Stress field for the eastern Betic Cordillera, according to Alfaro et al. (1999) and Coca and Buforn (1994) respectively; 7.– Stress field for the Alboran Sea according to Udías et al. (1976), Buforn et al. (1995) and Bezzeghoud and Buforn (1999). 8 and 9.– Stress field for the Betic zone from reverse and normal faults, respectively, according to Galindo et al. (1999). 10.– Stress field for the zone corresponding to the Azores-Gibraltar fault according to Moreira (1985), Grimison and Chen (1986), Buforn et al. (1988a), Udías and Buforn (1991) and Galindo Zaldívar et al. (1993). 11.– Stress field for the North of Africa according to Udías (1982), Medina and Cherkaoui (1991), Udías and Buforn (1991) and Bezzeghoud and Buforn (1999). Grey and black arrows without numbers represent trends of the regional maximum horizontal stress trajectories (data from northern and central Spain has been taken from Cortés and Maestro, 1998, and Herraiz et al., 2000). It is possible to see two superimposed stress fields in the Pyrenees and southwards (grey arrows and small, black arrows indicate the two stress fields determined by Cortés and Maestro, 1998). Plate boundary line according to Udías and Buforn (1991). Pole of rotation between Africa and Eurasian plates according to Buforn et al. (1988b). Open arrows show the relative movement between the Eurasian and African plates.

continental subduction (Morales et al., 1999). Many of these hypotheses share part of their conclusions.

The stress field existing in various sectors of this region has been described in numerous previous studies (Figure 1). For the Azores-Gibraltar sector, where the earthquakes of greatest magnitude of the region occur, the P axis is oriented NW-SE to NNW-SSE and the T axis is horizontal, trending NE-SW to ENE-WSW (Moreira, 1985; Grimison and Chen, 1986; Buforn et al., 1988a; Udías and Buforn, 1991; Galindo-Zaldivar et al., 1993). Similar orientation has been observed in the North of Africa (Udías, 1982; Medina and Cherkaoui, 1991; Udías and Buforn, 1991; Bezzeghoud and Buforn, 1999).

The rotation pole of the African and European plates is located close to the Canary Islands. According to the NUVEL-1 model (DeMets et al., 1990, 1994), the velocity of displacement of Africa with respect to Europe is around 7 mm/year in the north of Algeria, diminishing toward the west to 4 mm/year in the Atlantic Ocean. The displacement direction changes progressively through this region, rotating from a NNW-SSE direction in the north of Algeria, to NW-SE in the Alboran Sea and Gulf of Cadiz, and E-W in the Atlantic Ocean (Figure 1). Previous seismological data indicate the same progressive variation of the orientation of the principal stress field in the study area.

In the south of the Iberian Peninsula and Alboran Sea the situation is highly complex, as a result of a diffuse, low-magnitude seismicity, which corresponds to shallow, intermediate and deep earthquakes. Based on the shallow earthquakes, the study area is subject to NW-SE to N-S horizontal compression (Buforn et al., 1988b; Coca and Buforn, 1994; Buforn et al., 1995; Mezcua and Rueda, 1997; Proyecto Sigma, 1998; Herraiz et al., 2000). The results obtained with the intermediate seismicity show variations depending on the author and the data used in the analysis. Accordingly, Griminson and Chen (1986) determined an E-W-trending compression, while Buforn et al. (1991) obtained compression trending NW-SE to E-W and dipping 45°. Galindo et al. (1993) indicated the existence of a subhorizontal compression trending WNW-ESE and tension towards the NNE with small dipping. Morales et al. (1999) observed a variation in the orientation of the stress field with depth: for the shallower earthquakes (40 km $\leq$ h $\leq$ 80 km) they observed NW-SE compression, which could be horizontal or dipping towards the NW, and vertical tension. For deeper earthquakes (65 km $\leq$ h $\leq$ 100 km) the compression is vertical and the tension horizontal in a NW-SE direction. For the very deep earthquakes there is E-W compression dipping 45° to the E (Udías et al., 1976; Buforn et al., 1991) and tension dipping to the W (Galindo et al., 1993).

According to these previous results there is no clear definition of the orientation of the stress field that is operating over the Ibero-Maghrebi region. This is partly due to the complex geological context and partly to the fact that many of the studies referred to focussed only on particular areas within the region, and so used only a part of the available information. Here, we present the results obtained from the application of the right dihedron method (Pegora, 1972; Angelier and Mechler, 1977) to the whole region, as well as to various separate sectors within it. To achieve this a catalogue of focal mechanisms, updated to December 2000, was used, which integrated and standardized the results provided by different authors and agencies (Henares et al., 2000; Henares and López Casado, 2001).

Data

The cited catalogue consists of 486 solutions, of which 453 correspond to individual and 33 to joint solutions. Of the individual solutions, 400 are surface earthquakes, 50 are intermediate and 3 are very deep. The magnitude of the earthquakes in the catalogue varies between 1.2 and 8.2. Information about the earthquakes in this catalogue were standardized, based on the earthquake catalogue of the Instituto Geográfico Nacional (IGN) updated to the year 2000. Information about mechanisms was completed and standardized with respect to the notation of the angles representing the planes and the axes of the focal mechanisms.

Earthquakes with a magnitude $>$ 5.0 were used in this study when the region as a whole was considered; magnitudes $\geq$ 5.0 when the region was divided in four sectors, and $\geq$ 4.0 when the region was divided into the southern Iberian Peninsula and northern Morocco. These values were chosen to try and ensure that the results have real tectonic significance.

To ensure the quality of the plane solutions used, the number of observations (N) was $\geq$ 10, wherever possible. Accurate locations of the earthquakes were determined using minimum values of RMS (the root mean square travel time residual, measured in seconds), ERH (standard deviation of the epicentre solution, in km) and ERZ (standard deviation of the depth solution, in km). These minimum error conditions varied depending on the individual study zone (see Tables 3, 4 and 5). Tables 1 and 2 present the 130 solutions used in this study, selected according to the above quality and accuracy criteria and classified according to the different sectors considered.

For shallow earthquakes we used solutions from the P wave first motion methodology (Brillinger et al., 1980; Giner Robles, 1996) or from the wave-modelling methodology (MO). In the first case, a criterion of N $\geq$ 10 was chosen to ensure a minimum-acceptable azimuthal coverage. This restriction is not true mainly for the earliest earthquakes and the offshore ones. The P-wave first motion solutions comprise 72% of the total used. Of these, their score or number of successes in true polarities is known in more than 83% of cases, and in more than 90% of cases the score is greater than 0.75. The remaining solutions do not yield this information. The number

Table 1. Data used in Figure 2

Date	Lon.	Lat.	h	mb*	ϕ_1	δ_1	λ_1	ϕ_2	δ_2	λ_2
20/05/1931	16 30.0W	37 36.0	0	7.1	299	68	150	197	63	25
25/11/1941	19 01.0W	37 25.0	0	8.2	69	54	30	178	66	140
12/02/1946	4 57.0E	35 45.0	0	5.6	100	70	12	194	79	160
19/05/1951	3 56.0W	37 35.0	0	5.1	248	66	–33	353	60	–152
09/09/1954	1 28.0E	36 17.0	0	6.7	254	30	100	86	61	84
10/09/1954	1 18.0E	36 36.0	0	6.0	134	82	–180	44	90	–8
20/02/1957	9 00.0E	36 24.0	0	5.6	63	66	4	155	86	158
23/08/1959	3 13.6W	35 30.8	20	5.4	276	70	153	25	49	44
07/11/1959	2 30.0E	36 24.0	0	5.1	203	10	–5	298	89	–100
21/02/1960	4 15.0E	35 39.1	5	5.5	270	26	39	36	74	111
29/02/1960	9 37.0W	30 27.0	0	6.0	259	66	92	84	24	85
15/03/1964	7 45.0W	36 07.9	30	6.2	166	59	151	60	65	35
01/01/1965	4 30.0E	35 42.0	0	5.2	100	70	12	194	79	160
05/06/1965	1 30.0E	36 18.0	0	6.2	172	56	–32	281	64	–141
28/02/1969	10 48.8W	35 59.1	20	7.3	97	54	58	231	47	126
28/02/1969	10 42.0W	36 12.0	0	5.7	62	54	107	270	39	68
05/05/1969	10 24.0W	36 00.0	0	5.5	108	80	50	210	41	165
06/09/1969	12 18.0W	36 54.0	0	5.7	84	82	–169	352	79	–8
24/12/1969	10 30.0W	36 00.0	0	5.1	92	74	146	351	57	160
30/12/1970	14 48.2W	37 10.2	20	5.1	68	80	73	188	19	149
24/11/1973	4 24.0E	36 06.0	17	5.1	70	86	–176	340	86	–4
24/11/1973	4 24.0E	36 06.0	0	5.1	200	90	–14	290	76	–180
26/05/1975	17 36.0W	35 54.0	0	6.7	287	76	–180	197	90	–14
26/05/1975	17 33.6W	36 02.4	0	5.5	58	64	–148	313	62	–29
07/08/1975	4 35.5W	36 24.9	28	5.2	186	42	52	321	57	118
28/08/1977	8 12.6E	38 12.6	15	5.1	258	29	76	62	62	98
12/01/1979	17 11.4W	35 33.0	5	5.3	217	37	–28	330	74	–124
08/12/1979	11 29.4E	37 57.0	15	5.4	235	45	114	87	50	68
10/10/1980	1 26.8E	36 09.2	5	6.5	225	54	97	57	36	80
10/10/1980[1]	1 26.8E	36 09.2	10	6.5	210	45	90	30	45	90
10/10/1980	1 38.9E	36 10.0	5	6.2	58	43	98	250	47	82
13/10/1980	1 40.7E	36 22.7	5	5.2	63	42	112	271	51	72
30/10/1980	1 41.6E	36 22.9	5	5.1	186	46	140	66	63	51
08/11/1980	1 26.8E	36 12.0	5	5.3	231	31	83	43	60	94
07/12/1980	1 15.1E	35 57.5	5	5.5	277	40	39	39	66	123
01/02/1981	1 45.9E	36 27.0	11	5.5	210	43	116	64	52	68
17/10/1983	17 27.0W	37 38.8	16	6.0	58	85	72	163	19	164
26/05/1985	4 38.3W	37 47.2	5	5.1	20	48	61	160	50	119
27/10/1985	6 45.0E	36 29.0	10	5.5	240	80	175	149	85	10
31/10/1988	2 36.5E	36 26.6	13	5.4	103	55	14	201	79	144
29/10/1989	2 26.0E	36 44.9	5	5.7	245	66	91	68	24	87
12/03/1992	2 31.9W	35 16.3	8	5.3	173	72	–15	268	76	–162
12/06/1992	8 29.7E	34 19.6	8	5.3	60	75	–160	325	72	–16
23/10/1992	4 21.4W	31 13.2	7	5.3	187	69	166	92	77	22
30/10/1992	4 23.0W	31 24.7	21	5.1	90	72	3	181	87	162
23/05/1993	2 25.5W	35 16.4	6	5.4	308	84	179	218	89	6
26/05/1994[2]	3 52.0W	35 08.0	7	5.3	330	77	–45	73	46	–162
26/05/1994	4 00.0W	35 15.9	3	5.7	355	69	177	264	88	21
18/08/1994	0 08.5W	35 28.7	5	5.7	58	45	86	232	45	94
22/12/1999	1 13.2W	35 10.2	12	5.5	221	57	100	59	34	75
10/11/2000	4 54.0 E	36 25.8	18	5.8	239	65	89	57	25	92

h: depth; mb* macroseismic mb when mb > 6.5; azimuth (ϕ), dip (δ) and slip (λ): solution of principal and auxiliary planes.
[1] The earthquake 10/10/80 of magnitude 6.5 is composed of two subevents (Yielding et al., 1981). This is the second subevent.
[2] The earthquake 26/05/94 of magnitude 5.7 is composed of two subevents (Bezzeghoud and Buforn, 1999). This is the first subevent.

Table 2. Data used in figures 3, 4 and 5

Date	Lon.	Lat.	h	mb*	ϕ_1	δ_1	λ_1	ϕ_2	δ_2	λ_2
Figure 3-Sector 1										
20/05/31	16 30.0W	37 36.0	0	7.1	299	68	150	197	63	25
25/11/41	19 01.0W	37 25.0	0	8.2	69	54	30	178	66	140
15/03/64	7 45.0W	36 07.9	30	6.2	166	59	151	60	65	35
28/02/69	10 48.8W	35 59.1	20	7.3	97	54	58	231	47	126
17/10/83	17 27.0W	37 38.8	16	6.0	58	85	72	163	19	164
Figure 3-Sector 1a										
20/05/31	16 30.0W	37 36.0	0	7.1	299	68	150	197	63	25
25/11/41	19 01.0W	37 25.0	0	8.2	69	54	30	178	66	140
17/10/83	17 27.0W	37 38.8	16	6.0	58	85	72	163	19	164
Figure 3-Sector 1b										
06/09/69	12 18.0W	36 54.0	0	5.7	84	82	–169	352	79	–8
30/12/70	14 48.2W	37 10.2	20	5.1	68	80	73	188	19	149
Figure 3-Sector 1c										
15/03/64	7 45.0W	36 07.9	30	6.2	56	71	5	276	24	53
28/02/69	10 48.8W	35 59.1	20	7.3	97	54	58	231	47	126
28/02/69	10 42.0W	36 12.0	0	5.7	62	54	107	270	39	68
05/05/69	10 24.0W	36 00.0	0	5.5	108	80	50	210	41	165
20/12/89	7 23.5W	37 13.5	23	5.0	259	80	13	351	77	170
Figure 3-Sector 2										
12/03/92	2 31.9W	35 16.3	8	5.3	60	75	–160	325	72	–16
23/05/93	2 25.5W	35 16.4	6	5.4	308	84	179	218	89	6
26/05/942	3 52.0W	35 08.0	7	5.3	330	77	–45	73	46	–162
26/05/94	4 00.0W	35 15.9	3	5.7	355	69	177	264	88	21
Figure 3-Sector 3										
24/06/84	3 44.3W	36 50.3	5	5.0	100	83	25	193	66	172
13/09/84	2 20.5W	36 58.9	9	5.0	228	46	156	121	73	47
26/05/85	4 38.3W	37 47.2	5	5.1	20	48	61	160	50	119
23/12/93	2 56.2W	36 46.8	8	5.0	300	70	–130	188	44	–29
Figure 3-Sector 4										
10/10/80	1 26.8E	36 09.2	5	6.5	225	54	97	57	36	80
10/10/80[1] 1	1 26.8E	36 09.2	10	6.5	210	45	90	30	45	90
10/10/80	1 38.9E	36 10.0	5	6.2	58	43	98	250	47	82
13/10/80	1 40.7E	36 22.7	5	5.2	63	42	112	271	51	72
30/10/80	1 41.6E	36 22.9	5	5.1	186	46	140	66	63	51
08/11/80	1 26.8E	36 12.0	5	5.3	231	31	83	43	60	94
05/12/80	1 23.0E	35 58.5	5	5.0	112	61	–179	22	89	–29
07/12/80	1 15.1E	35 57.5	5	5.5	277	40	39	39	66	123
15/01/81	1 39.1E	36 26.3	11	5.0	181	53	150	72	67	41
01/02/81	1 45.9E	36 27.0	11	5.5	210	43	116	64	52	68
15/11/82	1 26.1E	35 40.6	7	5.0	274	70	–169	180	80	–20
05/03/85	1 28.3E	35 38.4	9	5.0	225	54	83	33	37	100
27/10/85	6 45.0E	36 29.0	10	5.5	240	80	175	149	85	10
31/10/88	2 36.5E	36 26.6	13	5.4	103	55	14	201	79	144
29/10/89	2 26.0E	36 44.9	5	5.7	245	66	91	68	24	87
18/08/94	0 08.5W	35 28.7	5	5.7	58	45	86	232	45	94
22/12/99	1 13.2W	35 10.2	12	5.5	221	57	100	59	34	75
10/11/00	4 54.0 E	36 25.8	18	5.8	239	65	89	57	25	92
16/11/00	4 46.2 E	36 45.6	18	5.0	294	85	45	29	45	173
Figure 4-Sector 1c										
05/12/60	6 37.3W	35 41.4	5	4.9	73	86	–178	343	88	–4
15/03/64	7 45.0W	36 07.9	30	6.2	56	71	5	276	24	53
28/02/69	10 48.8W	35 59.1	20	7.3	97	54	58	231	47	126
28/02/69	10 42.0W	36 12.0	0	5.7	62	54	107	270	39	68
05/05/69	10 24.0W	36 00.0	0	5.5	108	80	50	210	41	165
18/04/72	11 09.8W	36 25.8	20	4.7	99	80	–155	8	65	–2
20/12/89	7 23.5W	37 13.5	23	5.0	259	80	13	351	77	170
04/07/94	6 58.4W	37 34.4	21	4.1	88	53	75	244	40	109
Figure 4-Sector 2										
29/04/73	3 59.3W	34 33.8	10	4.6	212	90	1	122	90	180
14/07/74	3 41.0W	35 33.5	5	4.4	36	89	0	126	89	–180
07/04/81	4 00.2W	35 06.9	8	4.0	182	75	132	76	44	22
09/12/87	3 49.2W	35 25.4	7	4.3	54	49	–58	190	50	–123
05/10/88	3 53.6W	35 30.1	11	4.0	248	26	–58	32	68	–105
12/03/92	2 31.9W	35 16.3	8	5.3	60	75	–160	325	72	–16
23/05/93	2 25.5W	35 16.4	6	5.4	308	84	1	218	89	174
26/05/94[2]	3 52.0W	35 08.0	7	5.3	330	77	–45	73	46	–162
26/05/94	4 00.0W	35 15.9	3	5.7	355	69	177	264	88	21
Figure 4-Sector 3a										
20/03/79	3 48.1W	37 09.8	5	4.1	316	78	–179	225	87	–12
03/12/80	5 40.4W	36 55.1	27	4.3	217	61	155	114	68	32
21/01/81	4 42.6W	36 51.3	5	4.0	153	56	134	33	53	44
24/06/84	3 44.3W	36 50.3	5	5.0	100	83	25	193	66	172
26/04/86	3 43.3W	37 13.1	5	4.0	10	22	64	162	70	100
05/12/88	3 50.4W	37 00.5	7	4.0	100	58	53	225	47	134
07/11/90	3 42.0W	36 59.3	2	4.0	315	90	–90	135	0	–90
Figure 4-Sector 3b										
26/05/85	4 38.3W	37 47.2	5	5.1	20	48	61	160	50	119
26/05/85	4 36.3W	37 49.2	5	4.5	210	35	29	324	73	122
11/03/87	3 23.8W	37 43.6	6	4.3	235	48	61	15	50	119
16/04/96	4 39.5W	37 36.9	8	4.3	75	76	–179	345	89	–14
Figure 4-Sector 3c										
25/10/79	0 46.1W	38 00.8	20	4.2	150	83	–170	59	81	–7
05/03/81	0 12.9E	38 29.6	20	4.9	15	65	–48	130	48	–145
14/08/91	0 57.6W	38 45.3	2	4.1	317	78	–174	226	85	–12
26/11/95	1 16.2W	38 02.3	2	4.1	324	71	–162	228	73	–20
02/02/99	1 30.0W	38 09.0	4	4.8	38	76	–10	131	80	–166
Figure 4-Sector 3d										
06/06/77	1 43.7W	37 38.7	9	4.2	210	46	–116	65	50	–66
14/05/79	2 27.5W	37 36.3	5	4.2	107	49	–40	226	61	–131
20/03/83	2 12.1W	36 32.8	6	4.4	5	74	–151	266	62	–18
06/01/83	2 09.2W	36 29.6	12	4.7	66	78	33	163	58	166
13/09/84	2 20.5W	36 58.9	9	5.0	228	46	156	121	73	47
08/11/94	2 19.3W	36 55.0	6	4.0	340	17	119	130	75	98
07/06/95	2 10.6W	36 55.7	7	4.0	120	65	–132	5	48	–35
18/11/95	2 31.8W	36 54.9	3	4.0	130	80	–45	230	45	–166
02/09/96	1 33.0W	37 33.5	1	4.5	61	63	–13	157	78	–152
Figure 4-Sector 3e										
23/12/93	2 56.2W	36 46.8	8	5.0	300	70	–130	188	44	–29
04/01/94	2 48.9W	36 34.3	2	4.9	130	55	23	234	70	143
02/07/97	3 15.2W	36 25.7	2	4.4	193	25	120	46	69	77
02/07/97	3 13.4W	36 22.0	0	4.2	191	35	111	36	58	76
Figure 5-Sector 1										
13/02/85	4 01.9W	36 55.2	30	2.9	355	12	–2	87	89	–102
13/01/86	4 08.0W	37 13.0	27	3.6	269	72	2	360	89	162
02/04/92	3 51.3W	37 05.9	24	3.3	23	45	–117	239	51	–65
04/05/94	4 13.2W	37 14.4	21	3.0	97	65	–90	277	25	–90
18/12/95	3 47.0W	37 27.0	25	3.4	340	60	180	250	90	30
Figure 5-Sector 2										
06/08/84	4 08.9W	37 05.1	41	3.2	185	32	–162	79	80	–60
19/11/85	4 14.3W	36 44.3	55	3.1	330	63	–103	123	30	–114
25/08/91	4 29.0W	36 49.1	58	3.8	242	60	6	335	85	150
17/03/95	4 20.3W	36 49.5	56	4.0	246	84	74	356	17	159
18/11/95	4 19.0W	37 01.0	52	3.6	226	58	67	7	39	122
05/12/95	4 31.4W	36 48.5	56	3.1	252	82	–85	40	9	–122
Figure 5-Sector 3										
13/06/74	4 07.3W	36 52.5	60	4.1	78	72	–69	207	27	–138
27/03/87	4 05.7W	36 47.1	69	3.5	231	16	110	72	75	84
01/12/88	4 20.3W	36 50.3	67	3.2	15	45	141	255	63	52
03/09/92	4 26.8W	36 35.8	71	3.5	299	41	–60	82	55	–113
28/11/95	4 22.7W	36 41.8	68	3.5	230	45	110	77	48	71
20/08/97	4 44.2W	36 23.0	65	4.2	103	85	–99	344	10	–29
Figure 5-Sector 4										
10/09/88	4 24.6W	36 21.1	90	3.0	197	56	–121	64	45	–53
12/12/88	4 34.3W	36 17.0	95	4.5	316	50	175	222	86	40
19/07/89	4 25.5W	36 38.2	95	3.0	134	12	29	296	79	94
02/05/90	4 31.3W	36 31.9	95	4.2	45	23	128	265	72	75
18/11/90	4 35.1W	36 24.7	85	3.4	175	51	–30	285	67	–137
Figure 5-Sector 5										
30/05/88	4 36.1W	36 25.4	100	3.5	166	55	178	75	89	35
28/11/88	4 34.1W	36 18.0	100	3.5	205	5	–157	93	88	–85
Figure 5-Sector 6										
22/06/80	5 19.3W	35 59.2	80	4.7	304	66	–135	192	50	–32
13/04/90	4 48.9W	35 36.5	89	3.9	263	53	135	142	56	47
28/09/90	4 32.7W	35 57.7	113	3.7	306	76	77	83	19	131
Figure 5-Sector 7										
17/04/68	3 44.8W	35 17.1	22	5.0	81	79	–177	350	87	–11
10/02/80	4 57.7W	35 17.4	20	3.2	55	85	–18	147	72	–175
01/05/93	6 19.9W	35 17.4	30	4.2	15	25	–60	162	69	–103
Figure 5-Sector 8										
30/01/73	3 44.4W	36 51.2	660	4.0	303	37	–153	191	74	–56
08/03/90	3 32.6W	36 54.7	627	4.8	0	28	–88	177	62	–91
08/03/90[3]	3 32.6W	36 54.7	627	4.8	188	56	165	89	77	35

[1,2] and mb* See Table 1.

[3] The earthquake 08/03/90 of magnitude 4.8 is composed of two subevents (Buforn et al. 1997). This is the second subevent.

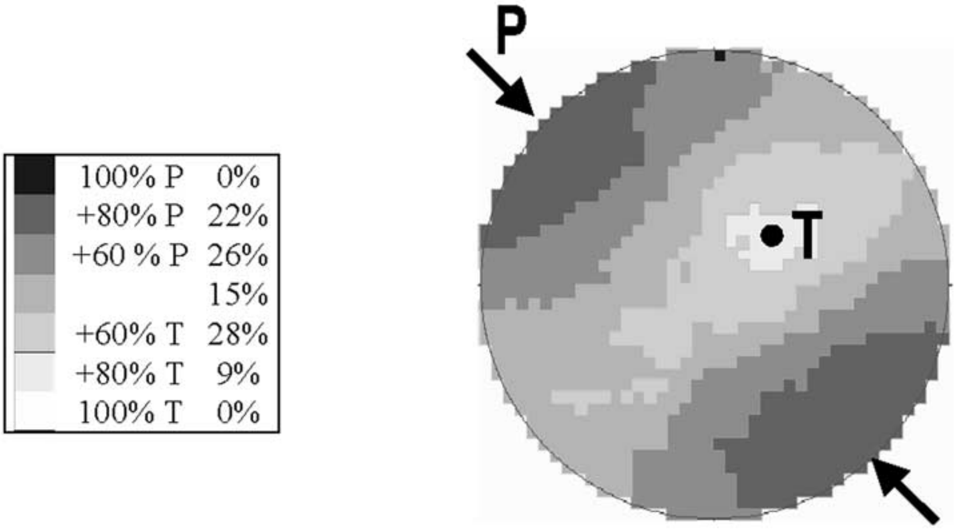

Figure 2. Diagram obtained using the right dihedron method for the entire study area, considering the earthquakes represented in table 1. Key to colours: A) 100% P; B) +80% P; C) +60% P; D) 60% P–60% T; E) +60% T; F) +80% P; G) 100% T. (P: Pressure; T: Tension).

of observations was not considered as a restriction in the solutions calculated using the MO methodology. An unusual case is the diagram presented for sector 3 in Figure 3. In this sector only one solution was calculated with the P wave first motion and the remaining were calculated by inversion of the moment tensor or by wave-form modelling methods. The solutions of deep and very deep earthquakes were obtained using only the first motion of the P wave.

Methods

The stress field of the Iberian-Maghrebi area was obtained by studying the focal mechanisms and using the right-dihedron method. This method can be applied to a group of faults or a group of focal mechanisms (this latter in our case). In both cases the stereographic projections are superimposed in order to identify compatible areas of extension and compression. These areas are classified according to the percentage compatibility of the compression and extension obtained. The absence of areas with 100% compatibility may be due to measurement errors, errors in the determination of the mechanisms, or faults or mechanisms belonging to different stress regimes. If the area where the compression or extension is 100% compatible is large, the results will only be approximate. In contrast, if these areas are small and the P and T axes are perpendicular, the results will be of very good quality. To use this geometric method, the seismotectonic region must have an homogeneous stress tensor. If it does not, subregions need to be defined using other criteria to obtain the different stress tensors. Finally, those solutions with the worse fit are rejected and a similar process followed with the different solutions of each earthquake.

To find the stress tensor of the whole region we first considered shallow earthquakes with $m_b > 5.0$ (Figure 2). A stress field with a horizontal P axis in a NW-SE direction and approximately vertical T axis was obtained. In both cases we obtained more than 80% compatibility. In addition, for the compression, there is a very small, north-trending area with 100% compatibility. To continue our study the area was divided into four sectors according to the distribution of the earthquakes and the different geological domains concerned (Figure 3). These sectors are: 1) from the Azores to Gibraltar, along the contact between the African and Eurasian plates (this area has been divided into three sectors according to the results of the NUVEL-1 model), 2) northern Morocco, including part of the Alboran Sea (Rif domain affected by NE-SW faults), 3) the Betic Mountain range, with several earthquakes situated in the north of the Alboran Sea, but near the southern coast of Spain, and 4) northern Algeria and Tunisia (Tell Mountain range).

With respect to the shallow earthquakes with $m_b \geq 4.0$, area 3 in Figure 3 was subdivided into several zones (Figure 4) according to the existing earthquake grouping, ensuring at the same time that these cor-

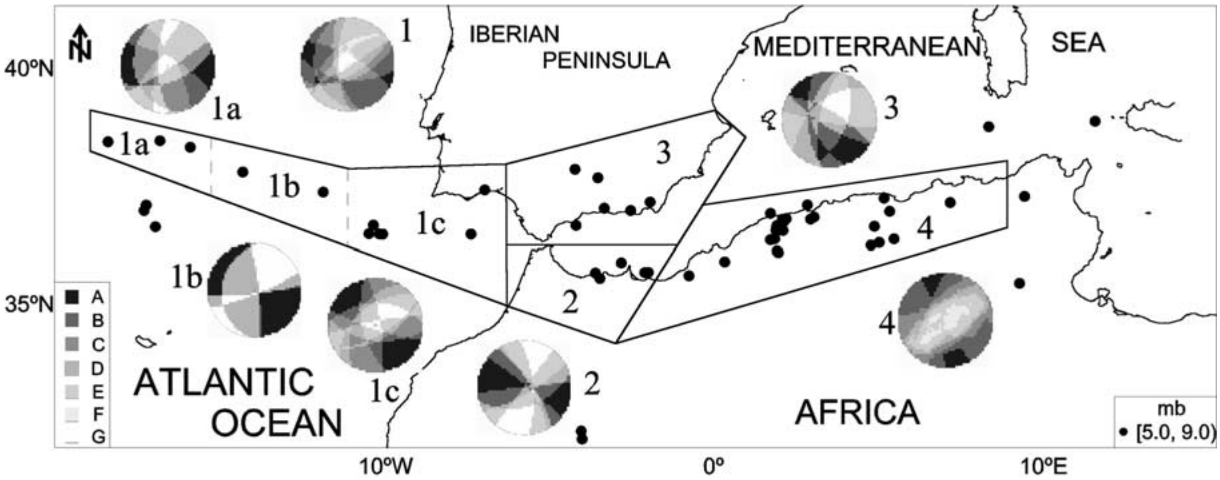

Figure 3. Diagrams obtained using the right dihedron method for earthquakes in the Iberian-Maghrebi region having a magnitude $m_b \geq 5.0$. The various sectors considered in the analysis are shown and the diagrams obtained for each zone. Earthquakes used in the analysis with $m_b \geq 5.0$ are also shown. The earthquakes outside of the sectors were used together with those inside in the evaluation of the diagram in Figure 2. Key to colours: A) 100% P; B) +80% P; C) +60% P; D) 60% P–60% T; E) +60% T; F) +80% P; g) 100% T. (P: Pressure; T: Tension).

respond to areas with a high degree of geological homogeneity. The central part of the Betic Cordillera was divided into two zones: one (3a) corresponding to the earthquakes situated in the Betic Internal Zone or its proximities, and the other (3b) in the northern part of the Betics, in the area of contact with the Iberian Massif. The eastern part of the Betic Cordillera, affected by the important NE-SW faults of Alhama de Murcia, Palomares and Carboneras (continuing into the Alboran Sea) was divided into three parts. The northern one (3c) corresponds to the area where the Alhama-Lorca Fault has been absorbed and other NNE-SSW trending faults are responsible for the seismicity (Alfaro et al., 1999). To the south is the area of the Alhama-Palomares-Carboneras faults (3d). These faults are crossed by other NW-SE faults when they pass offshore and it is for this reason that the area is considered separately (3e). The NE-SW faults cross the Alboran Sea, but the present earthquake record shows a clear discontinuity with the southern border of the Alboran Sea, which caused us to treat it as a separate area (area 2 in Figures 3 and 4). Some earthquakes were grouped by size (Figures 4 and 5). Only in one sector were the earthquakes separated into normal and reverse fault solutions (NF and IF, respectively), because results obtained from considering them jointly did not provide a consistent solution. Finally, intermediate and deep earthquakes were also studied, grouping them by depth (Figure 5).

Quality factor

To study the quality of the diagrams of the right dihedra we define the following factor:

$$QF = \left(\frac{Ex}{T}\right) * \left(\frac{Ang}{90°}\right) * (1.9196e^{-(0.0583 \cdot x)}) \quad (1)$$

This factor varies between 0 and 1, where *Ex* is the number of mechanisms that fit the stress field defined by the diagram, *T* is the total number of mechanisms used to obtain the diagram, *Ang* is the angle between P and T, and *x* is the% area subjected to compression or extension.

The first term in eq. (1) represents the compatibility between the mechanisms within the area. If there are areas with 100% compatibility (compression or extension) this term will be 1. The second term measures the deviation from the theoretical 90° angle between the P and T axes (Lisle, 1987). The third term defines the size of the area of compatibility. If we consider that P and T are at the centre of the compatible area then, if this area is small, we can assume that the compression or extension is perfectly determined; however, if the area is large, uncertainty will exist. The reason for using an exponential relationship is that the uncertainty increases exponentially with the size of the area. The term is set to 1 when 10% of the area is subject to compression or extension in the sphere, 0.5 when we have 25% and 0.1 when we have 50%, in a linear regression process between uncertainty and surface area. For areas of compression or tension of less than 10%

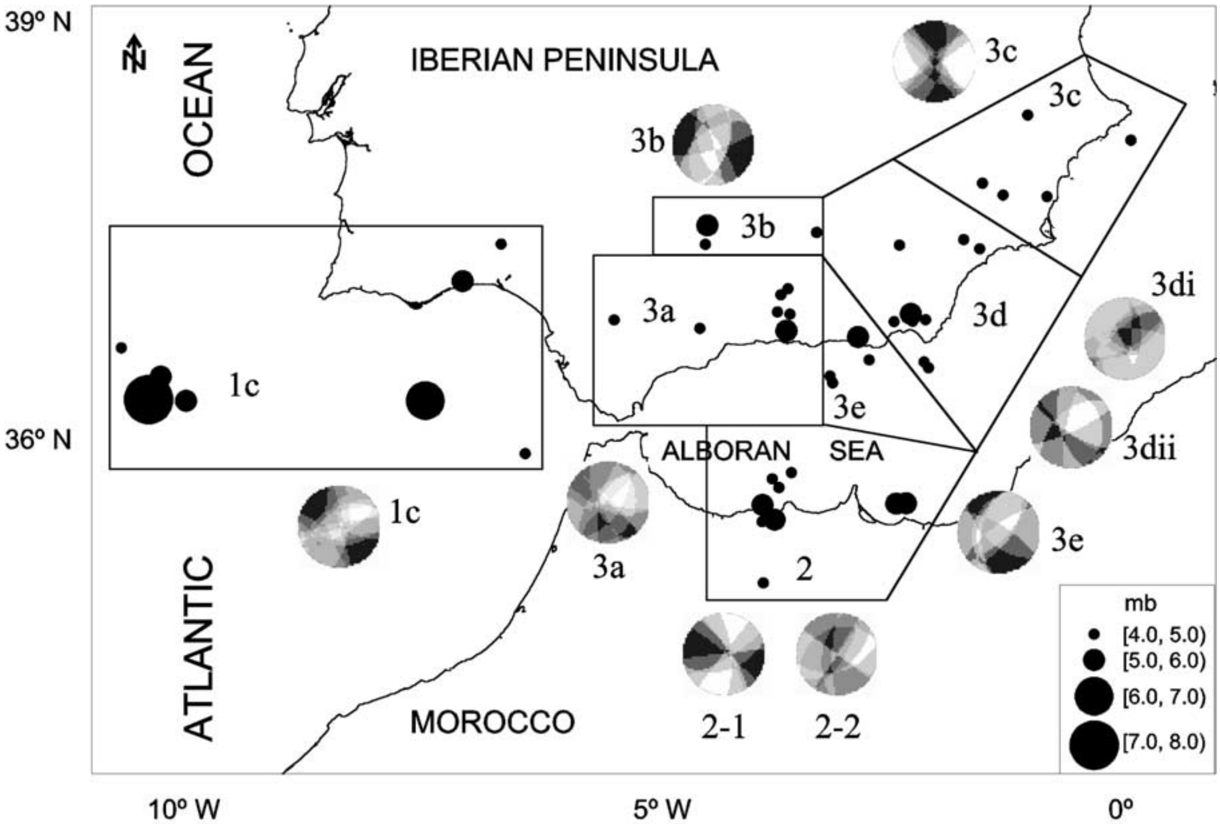

Figure 4. Diagrams obtained using the right dihedron method for earthquakes in the south of the Iberian Peninsula, Alboran Sea and northern Morocco, with magnitude $m_b \geq 4.0$. The sectors considered are: 1c) Gulf of Cadiz; 2) Alhoceima (here the earthquakes have been grouped by magnitude); 3a) Central-western Betic; 3b) Southern edge of the Iberian Massif; 3c) Prebetic-Murcia; 3d) Northern Almeria; 3e) Southern Almeria.

of the total area of the diagram, this term is set to 1. In cases where the two first terms of eq. (1) are equal to 1 but include very large areas of compression and/or extension, the position of the axes is poorly defined, and so QF is set to 0.25.

According to the value of this quality factor we classified the diagrams as very good [1–0.7], good [0.7–0.5], fair [0.5–0.3] and bad [0.3–0]. The results of this classification are given in Tables 3, 4 and 5, and show that 53.8% of the diagrams can be considered good or very good, while only 30.7% of the cases yield a poorer solution.

Results

The results obtained with all of the higher-magnitude earthquakes, $m_b > 5.0$ (Figure 2), show compression trending NW-SE for the entire region and an extension with moderate dipping towards the NE.

When the sectors differentiated within the study area are considered, a small variation to this general orientation is observed (Figure 3 and Table 3): there is a WNW-ESE compression in the area of the Azores-Gibraltar fault and a NW-SE compression in the Betic Cordillera, with an extension dipping towards the NE; in northern Algeria the direction of compression is NNW-SSE. In northern Morocco there is WNW-ESE compression and NNE-SSW extension. These results agree with the NUVEL-1 model (Figure 1) and with results obtained by other authors (Buforn et al., 1988a,b; Udías and Buforn, 1991; Galindo et al., 1993; Mezcua and Rueda, 1997; Proyecto Sigma, 1998; Bezzeghoud and Buforn, 1999). Sector 1 in Figure 3 can also be divided into three areas according to the results of the NUVEL-1 model. In Figure 3 sector 1a, there is E-W compression and vertical extension, in Figure 3 sector 1b the compression and the extension are poorly defined, and in Figure 3 sector 1c there is NW-SE compression and vertical extension. In

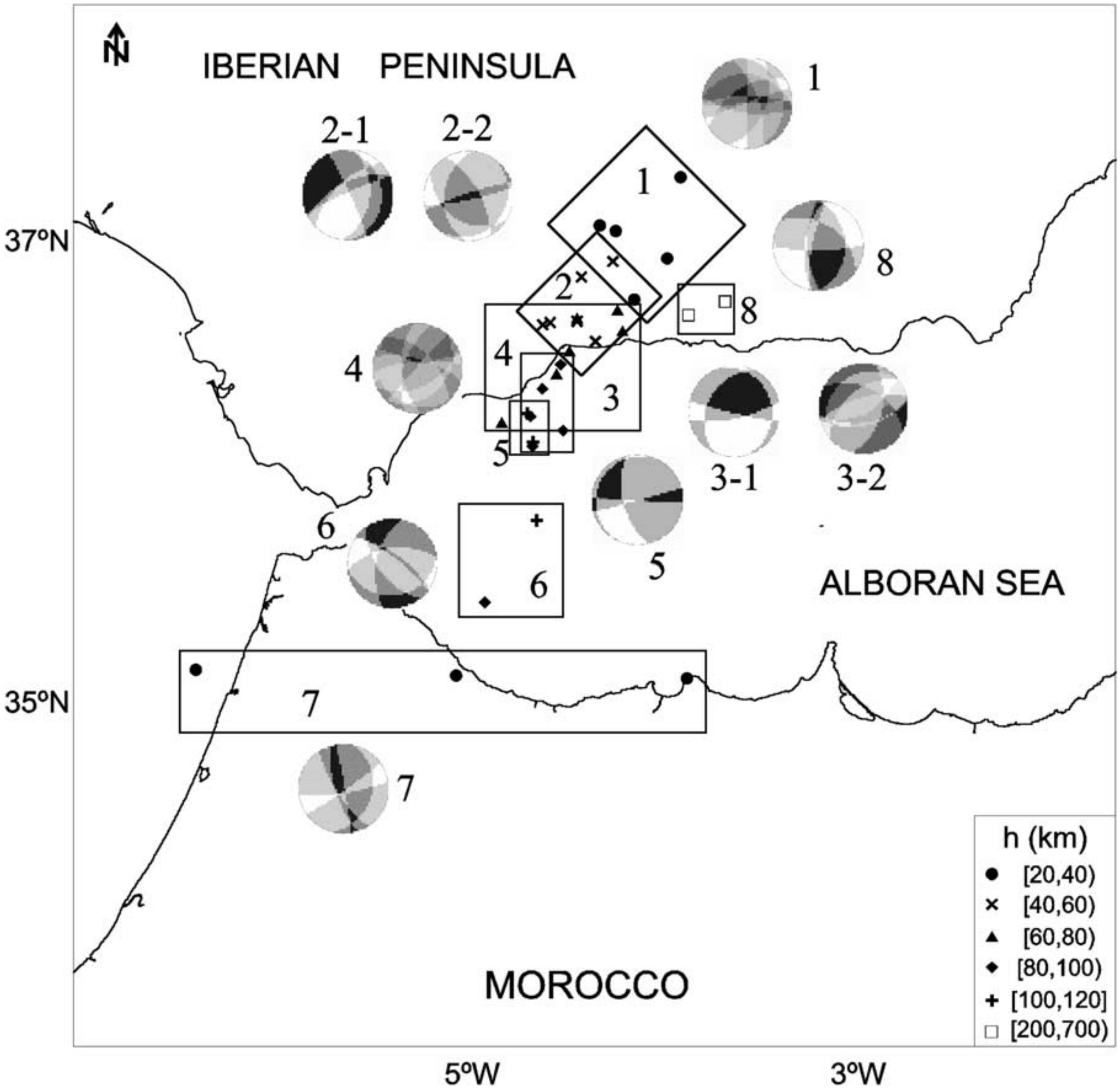

Figure 5. Diagrams obtained using the right dihedron method for intermediate (h = 20–120 km) and deep earthquakes (h > 600 km) in the south of the Iberian Peninsula and northern Morocco. The sectors correspond to the following depth ranges: 1) 20 km $\leq$ h $\leq$ 39 km; 2) 40 km $\leq$ h $\leq$ 59 km (here the earthquakes have been grouped by magnitude); 3) 60 km $\leq$ h $\leq$ 79 km (earthquakes grouped by magnitude); 4) 80 km $\leq$ h $\leq$ 99 km; 5) 100 km $\leq$ h $\leq$ 120 km; 6) Deep earthquakes in the area of the Strait of Gibraltar; 7) Deep earthquakes in northern Morocco; 8) h > 600 km.

the latter case, the earthquake of 24/12/1969 yields a solution that is not coherent with the stress state that defines the remaining focal mechanisms. This may be due to an erroneous plane solution or it may represent a local stress state. As a consequence it was excluded from the right-dihedra evaluation.

The results show greater dispersion in the Betic Cordillera and northern of Morocco when surface earthquakes of $m_b \geq 4.0$ (Figure 4; Table 4) are considered. In the north of the Gulf of Cadiz (Figure 4, sector 1c) there is a NW-SE compression and extension in the NE-SW direction, with moderate dipping to the NE. In this region the earthquakes of 24/12/1969 and 01/05/1993 were excluded since they did not fit the general stress state of the sector under consideration. Over a large part of the Alboran Sea and northern

Table 3. Stress field in the Iberian-Magrhrebi region from shallow earthquakes with magnitude $m_b \geq 5.0$

	Magnitude	RMS	ERH	ERZ	EQ	QF	P	T
Sector 1	[6.0, 8.2]				5	0.90	Subhorizontal N60–80W – S60–80E	Vertical
Sector 1a	[6.0, 8.2]				3	0.80	Subhorizontal N60–90W – S60–90E	Vertical or subhorizotal N0–15E – S0–15E
Sector 1b	[5.1, 5.7]				2	0.15	NW-SE not well defined	NE-SW not well defined
Sector 1c	[5.0, 7.3]				5	0.60	Subhorizontal N20–65W – S20–65E	N45E, dipping towards NE, or vertical
Sector 2	[5.3, 5.7]	≤ 0.9	≤ 4	≤ 5	4	0.38	Subhorizontal N55–90W – S55–90E	Subhorizontal N0–35E – S0–35W
Sector 3	[5.0, 5.1]	≤ 0.9	≤ 4	≤ 5	4	0.76	Subhorizontal trending N20–55W – S20–55E or with moderate dipping towards N190E	N35E, dipping towards NE
Sector 4	[5.0, 6.5]	≤ 1.2	≤ 8	≤ 10	19	0.88	Horizontal N0–30W – S0–30E	Subvertical or with moderate dipping towards N45E

RMS: The root mean square travel time residual, measured in seconds; ERH: Standard deviation of the epicentre solution, in km; ERZ: Standard deviation of the depth solution, in km; EQ: Number of earthquakes used in the analysis; QF: Quality factor.

Table 4. Stress filed in the Betic Cordillera and Alborán sea zones from shallow earthquakes of magnitude $m_b \geq 4.0$

	Magnitude	RMS	ERH	ERZ	EQ	QF	P	T
Sector 1c	[4.1, 7.3]				8	0.60	Subhorizontal N25–70W – S25–70E	N60E, dipping toward NE
Sector 2 (1)	[5.3, 5.7]	≤ 0.9	≤ 4	≤ 5	4		Subhorizontal N55–90W – S55–90E	Subhorizontal N0–35E – S0–35W
(2)	[4.0, 4.6]	≤ 1.1	≤ 3	≤ 8	5		N25W, dipping towards NNW	N55–90E, dipping towards ENE
Sector 3a	[4.0, 5.0]	≤ 1.3	≤ 5	≤ 6	7	0.67	N160W, dipping towards SW or subhorizontal N150E	N50E, dipping toward NE
Sector 3b	[4.3, 5.1]	≤ 0.9	≤ 5	≤ 6	4	0.40	N40–75W – S40–75E	Subvertical N175W
Sector 3c	[4.1, 4.9]	≤ 1.0	≤ 3	≤ 4	5	0.20	N20E-N30W – S20W-S30E	N60–125E – S60–125W
Sector 3d (i)	[4.0, 4.5]	≤ 1.1	≤ 6	≤ 11	6	0.57	Subvertical	N160E, dipping towards S, not well defined
(ii)	[4.0, 5.0]	≤ 1.1	≤ 6	≤ 11	3	1.00	Subhorizontal N50W – S50E or N105W dipping SW	N45–60E, dipping towards NE
Sector 3e	[4.2, 5.0]	≤ 0.9	≤ 2	≤ 2	4	0.25	Subhorizontal trending N0–45W – S0–45E	N45E, dipping toward NE

(i): Normal fault solution; (ii): Reverse fault solution.

Morocco (Figure 4, sector 2) the earthquakes were divided into two groups according to their magnitude. For the group with magnitudes of between 5.3 and 5.7 (Figure 4, sector 2–1), a WNW-ESE compression and a NNE-SSW extension is obtained. For the group with magnitudes of between 4.0 and 4.6 (Figure 4, sector 2–2) the direction of the maximum compression is subvertical and the extension is subhorizontal in the ENE-WSW direction. In the central part of the Betic Cordillera the results show a maximum compression close to NNW-SSE, subhorizontal or somewhat dipping towards the SE, and an extension oriented approximately perpendicular, ENE-WSW (Figure 4, sector 3a). The results along the southern edge of the Iberian Massif show WNW-ESE compression and a vertical extension (Figure 4, sector 3b).

In the eastern part of the Betic Cordillera the direction of the P axis is practically N-S, with a well-defined E-W extension (Figure 4, sector 3c). In the Cabo de Gata sector (Figure 4, sector 3d) and further to the north the solutions corresponding to normal and reverse faults had to be separated; as a result, an approximately NE-SW compression dipping towards the SW is observed only for the reverse solutions (Figure 4, sector 3dii). Finally, in the north-eastern part of the Alboran Sea, a NNW-SSE compression results, with a perpendicular extension, not unlike the position of the rest of the Alboran Sea (Figure 4, sector 3e).

Analysis of the earthquakes with an intermediate focal depth indicates that the orientation of the stress field is not well defined (Figure 5, Tables 2 and 5). Between 20–40 km depth the compression lies subvertically in the Betic cordillera (Figure 5, sector 1), but in

Table 5. Stress field obtained from intermediate and deep earthquakes

	Magnitude	Depth (km)	RMS	ERH	ERZ	EQ	QF	P	T
Sector 1	[2.9, 3.6]	[20, 40]	≤ 0.9	≤ 11	≤ 6	5	0.79	Subvertical	Horizontal not well defined
Sector 2 (1)	[3.6, 4.0]	[40, 60]	≤ 0.7	≤ 2	≤ 3	3	0.80	Subhorizontal trending N25–110W – S25–110E	N5–45E – S5–45W
(2)	[3.1, 3.5]		≤ 0.6	≤ 5	≤ 6	3	0.25	Subvertical	Horizontal not well defined
Sector 3 (1)	[3.7, 4.2]	[60, 80]	≤ 0.9	≤ 2	≤ 3	2		NNE, dipping towards NNE, not well defined	Not well defined
(2)	[3.2, 3.6]		≤ 0.7	≤ 2	≤ 3	4	0.61	Subhorizontal trending N60–100W – S60–100E	N45E, dipping toward NE
Sector 4	[3.0, 4.5]	[80, 100]	≤ 0.8	≤ 3	≤ 3	5	0.80	Subvertical	N155W, dipping toward SSW
Sector 5	3.5	[100, 120]	≤ 0.9	≤ 3	≤ 4	2	0.38	Subhorizontal trending N85E – S85W or NW-SE with moderate dipping towards NW (not well defined)	NE-SW, dipping towards SW, not well defined
Sector 6	[3.7, 4.7]	[80, 120]	≤ 1.0	≤ 2	≤ 6	3	0.52	Subhorizontal trending N10E-N30W – S10W-S30E	Subhorizontal trending N55–90W – S55–90E
Sector 7	[3.2, 5.0]	[20, 40]	≤ 0.9	≤ 5	≤ 13	3	0.25	N15W, variable dip	Subhorizontal trending N55–80E – S55–80W
Sector 8	[4.0, 7.0]	> 600	≤ 1.7	≤ 8	≤ 16	3	0.80	NNW-SSE, dipping towards SSE, not well defined	NE-SW, not well defined

northern Morocco it lies approximately N-S but with very variable dip (Figure 5, sector 7). Between 40 and 60 km the results depend on the interval of magnitudes considered; thus, for earthquakes with a magnitude m_b between 3.6 and 4.0, the compression is subhorizontal in an E-W to NW-SE direction, while the extension is orientated NE-SW and dips towards the SW (Figure 5, sector 2i). When smaller-magnitude earthquakes are considered ($3.1 \leq m_b \leq 3.5$), the compression is subvertical and the extension trends WNW-ESE or NNW-SSE (Figure 5. sector 2ii). Because all data are of similar quality (Table 5), this difference indicates that earthquakes with smaller magnitude tend to be influenced by local stress fields.

Similar orientations have been obtained for the earthquake mechanisms with focal depths of between 60 and 80 km (Figure 5, sector 3), although here the direction of maximum compression is closer to E-W. Between 80 and 100 km (Figure 5, sector 4) the compression is subvertical. Between 100 and 120 km depth (Figure 5, sector 5) the focal mechanisms have been calculated for two earthquakes only. As a consequence, the orientation of the stress field is poorly defined, and the directions of maximum compression are seen to lie: a) horizontally in an NE-SW direction with moderate dipping towards NW, b) vertically, and c) horizontally, trending NW-SE or NNW-SSE (similar to results presented by Grimison and Chen, 1986 and Buforn et al., 1991). Further to the south (Figure 5, sector 6), the mechanisms of earthquakes with focal depths of between 80 and 120 km show subhorizontal compression NNW-SSE, with the T axis lying perpendicularly.

The deep seismicity ($h > 600$ km) does not allow a clear definition of the orientation of the stress fields existing at this depth range. A NNW-SSE compression is deduced, with strong dipping towards the SSE, whilst the extension lies subhorizontally and is orientated NE-SW (Figure 5, sector 8).

Discussion

Analysis of the focal mechanisms of shallow earthquakes has shown the existence of general compression between Iberia and Africa trending approximately NW-SE (Figure 6). To the W and NW, the orientation of the compression tends to change to a WNW-ESE direction towards the Atlantic, as the stress field produced by the opening of the Atlantic becomes dominant (Figure 6). Whereas, in the Betic Cordillera and northern part of Alboran Sea, an approximately ENE-WSW extension is detected. The northern Algeria and Tunisia sector shows NNW-SSE compression.

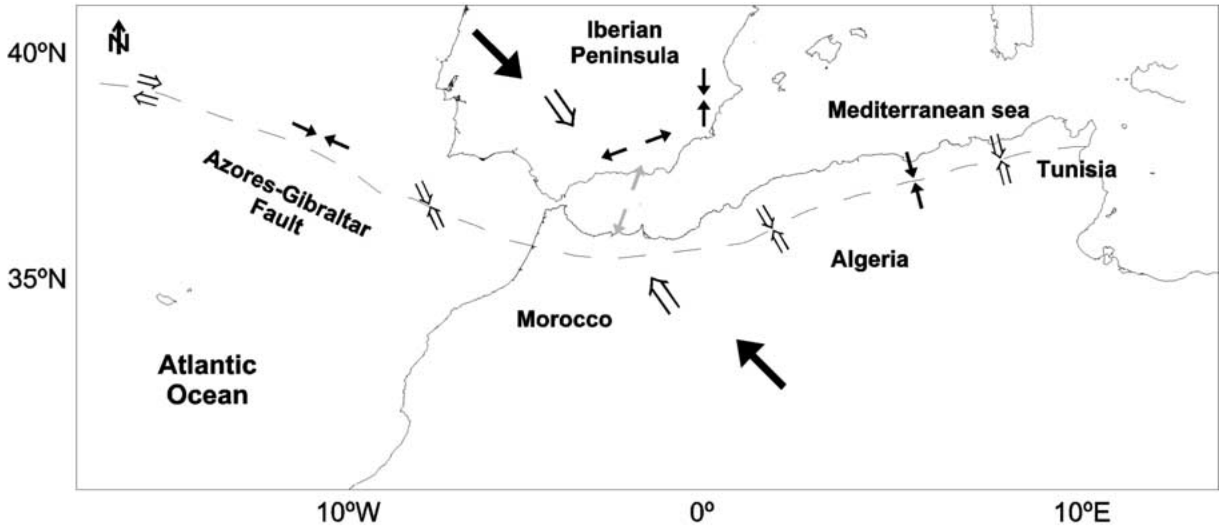

Figure 6. Stress field orientation in the study zone (solid arrows) (see discussion and conclusions). Open arrows show the relative movement between the Eurasian and African plates. Grey arrows indicate a possible extension of Alboran Sea.

The results obtained in the eastern sector of Betic Cordillera are almost N-S, in contrast to the NNW-SSE to WNW-ESE compression described above. The interpretation of this feature is problematical: it may be due to the scarcity of available data or to the fact that the orientation changes locally or to the presence of another stress field, as Cortés and Maestro (1998) indicated for areas further north. These authors found similar features in the Ebro Basin and surrounding areas, based on microtectonics data. In their opinion, it is due to the compression between Iberia and France, in the Pyrenees, which trends NNE-SSW and whose effects are also detected to the south. Similar results are given by Herraiz et al. (2000). It could be considered that such a field, induced by compression in the Pyrenees, might also have effects further south and that, in addition to local fields, the focal mechanisms of the earthquakes studied might indicate (depending on the geographic area): the approach of Iberia and Africa in the Rif and Betic Cordillera sectors, the opening of the Atlantic (WNW-ESE compression in the westernmost sectors of the region), and the effect of the compression between Iberia and the rest of Europe in the Pyrenees, which would give rise to a compression running N-S to NNE-SSW in the north-eastern part of the Betic (Figure 1).

In the southern part of Alboran Sea and northern Morocco sector some extension is also detected trending NNE-SSW, with perpendicular compression. This could be compatible with a certain continuity of the process that displaced the Internal Betic-Rif Zone towards the west at the same time as the continental crust was thinning.

In the Betic-Rif sector, it is possible to justify the proposed hypotheses about the present geodynamic framework. As commented previously, the extension obtained in the Alboran area is compatible with the movement of the Betic-Rif internal zone towards the west (Andrieux et al., 1971; Andrieux and Mattauer, 1973; Sanz de Galdeano, 1983, 1990, 1996, 1997; Galindo et al., 1999). Many studies propose the existence of subducted lithospheric laminae (Araña and Vegas, 1974; Blanco and Spackman, 1993). Using the focal mechanisms of seventeen intermediate earthquakes, Morales et al. (1999) proposed a continental subduction; however, when all the focal mechanisms of the intermediate and deep earthquakes included in the catalogue are considered, the results are very imprecise, with no clear directions of compression and extension being revealed. Buforn et al. (1997) considered the focal mechanisms of only ten intermediate earthquakes, and obtained a predominantly horizontal compression and mainly vertical tension; Mezcua and Rueda (1997), considering all of the focal mechanisms for the zone until that time, obtained a pressure, with small dipping, that changes progressively so that it is always perpendicular to the arc defined by the intermediate earthquakes found to the east of the Straits of Gibraltar; however, our results indicate that this occurs only in certain cases (Figure 5).

Examination of the present results confirms that the stress data proposed by the various previous articles can be partially justified. However, when all the mechanisms are considered the situation is not simple and must be imputed to the coexistence of several stress fields within the region. In fact geological data in this region show the coexistence of practically contemporary displacements of faults that in some cases are not compatible with a single stress field.

Buforn et al. (1995) proposed a process of subduction to explain the intermediate seismicity present in the region. In the Benioff zone, the compression is horizontal along-strike (e.g. Casacadia, Wang et al., 1995; Alaska, Lu et al., 1997), although in some models it can show deviations of down-dipping (Creager et al., 1995). Our situation is more complicated since, within the same depth interval, we find horizontal and vertical pressures (Figure 5). Therefore, it is not possible to conclude anything about the possible Benioff zone associated with this region.

Conclusions

The application of the right dihedron method to focal mechanisms of earthquakes of moderate and high magnitude ($m_b > 5.0$) which have occurred in the Iberian-Maghrebi region highlights the existence of a regional stress field with a subhorizontal P axis following the NW-SE direction. Superimposed on this field are more localised fields that are linked to the extension of the Atlantic Ocean and/or the interaction between the Eurasian, Iberian and African plates.

The results of sectors 1, 3, and 4 (Figure 3) agree well with those of the NUVEL-1 model. The remaining results do not agree with the NUVEL-1 model and indicate the possible existence of other stress fields in this area, distinct from those assumed by that model.

Interference between these fields is more evident in the context of the Betic Cordillera, Alboran Sea and northern Morocco, where the results are poorly defined, even for the mechanisms of the high-magnitude earthquakes recorded in these areas. The use of smaller-magnitude earthquakes allows an understanding of how the orientation of these fields varies, as well as a delimitation of the areas within which each one dominates.

On the basis of the intermediate seismicity, one can confirm that the results are imprecise and depend upon the depth interval and the geographical area under consideration. This lack of definition is undoubtedly a result of the aforementioned complex geodynamics of the region and to the fact that the data available is not yet sufficient. The various theories proposed to explain this seismicity are supported by part of the data used for this study and so only partially coincide with our results. New data will improve our understanding of this region.

Acknowledgements

This work was supported by the Dirección General de Enseñanza Superior e Investigación Científica (AMB97-0975-C02-01, PB97-1267-C03-01 and BTE2000-0339) and the Research Groups of the Junta de Andalucía RNM-0217, and Generalitat Valenciana GR00-22. We also acknowledge the revision and comments of the manuscript made by Mr P. Alfaro (U. Alicante).

References

Alfaro, P., Rueda, J., Delgado, J., Estévez, A., López Casado, C. and Giner, J., 1999, Sismotectónica de la cuenca del bajo Segura (Cordillera Bética central, Proc. 1^{a} Asamblea Hispano Portuguesa de Geodesia y Geofísica. Almeria. Ed. Universidad de Almería and Instituto Geográfico Nacional. España.

Andrieux, J., Fontboté, J.M. and Mattauer, M., 1971, Sur un modèle explicatif de l'Arc de Gibraltar, *Earth Plan. Sci. Lett.* **12**, pp. 191–198.

Andrieux, J. and Mattauer, M., 1973, Précisions sur un modèle explicatif de l'Arc de Gibraltar, *Bull. Soc. géol. France* **(7)XV**, pp. 115–118.

Angelier, J. y Mechler, P., 1977, Sur une méthode graphique de recherche des contraintes principales egalement utilisable en tectonique et en seismologie: la methode des diedres droites, *Bull. Soc. géol. France* **7**(19), 1309–1318.

Araña, V. and Vegas, R., 1974, Plate tectonics and volcanism in the strait of Gibraltar, *Tectonophysics* **24**, 197–212.

Bezzeghoud, M. and Buforn, E., 1999, Source Parameters of the 1992 Melilla (Spain, $M_W = 4.8$), 1994 Alhoceima (Morocco, $M_W = 5.8$), and 1994 Mascara (Algeria, $M_W = 5.7$) Earthquakes and Seismotectonic Implications, *Bull. Seism. Soc. Am.* **89**(2), 359–372.

Blanco, M.J. and Spackman, W., 1993, The P-wave velocity structure of the mantle below the Iberian Peninsula: Evidence for subduction lithophere below southern Spain, *Tectonophysics* **221**, 13–34.

Brillinger, D.R., Udías, A. and Bolt, B.A., 1980, A probability model for regional focal mechanism solutions, *Bull. Seism. Soc. Am.* **70**(1), 149–170.

Buforn, E., Udías, A. and Mezcua, J., 1988a, Seismicity and focal mechanisms in south Spain, *Bull. Seism. Soc. Am.* **78**(6), 2008–2024.

Buforn, E., Udías, A. and Colombás, M.A., 1988b, Seismicity, source mechanisms and tectonics of the Azores-Gibraltar plate boundary, *Tectonophysics* **152**, 89–118.

Buforn, E., Udías, A. and Madariaga, R., 1991, Intermediate and Deep Earthquakes in Spain, *Pageoph* **136**, núm. 4, 375–393.

Buforn, E., Sanz de Galdeano, C. and Udías, A., 1995, Seismotectonics of the Ibero-Maghrebian region, *Tectonophysics* **248**, 247–261.

Buforn, E., Coca, P., Udías, A. and Lasa, C., 1997, Source mechanism of intermediate and deep earthquakes in southern Spain, *J. Seismol.* **1**, 113–130.

Calvert, A., Sandvol, E., Seber, D., Barazangi, M., Vidal, F., Alguacil, G. and Jabour, N., 2000, Propagation of regional seismica phases (Lg and Sn) and Pn velocity structure along the Africa-Iberia plate boundary zone: tectonic implications, *Geophys. J. Int.* **142**, 384–408.

Coca, P. and Buforn, E., 1994, Mecanismos focales en el sur de España: Periodo 1965–1985, *Estudios Geológicos* **50**, 33–45.

Cortés, A.L. and Maestro, A., 1998, Recent intraplate stress field in the eastern Duero Basin (N Spain), *Terra Nova* **10**, 287–294.

Creager, C., Chiao, L.Y., Winchester, J.P., Engdahl, E.R., 1995, Membrane strain rates in the subducting plate beneath South America, *Geophys. Res. Lett.* **22**, 2321–2324.

DeMets, C., R. Gordon, D. Argus and S. Stein, 1990, Current plate motions, *Geophys. J. Int.* **101**, 425–478.

DeMets, C., R. Gordon, D. Argus and S. Stein, 1994, Effect of recent revisions to the geomagnetic reversal time scale on estimates of current plate motions, *Geophys. Res. Lett.* **21**, 2191–2194.

Galindo Zaldívar, J., González Lodeiro, F., and Jabaloy, A., 1993, Stress and palaeostress in the Betic-Rif cordilleras (Miocene to the present), *Tectonophysics* **227**, 105–126.

Galindo Zaldívar, J., Jabaloy, A., Serrano, I., Morales, J., González Lodeiro, F. and Torcal, F., 1999, Recent and present-day stresses in the Granada Basin (Betic Cordilleras): Example of a late Miocene-present-day extensional basin in a convergent plate boundary, *Tectonics* **18**(4), 686–702.

Giner Robles, J.L., 1996, Análisis Neotectónico y Sismotectónico en el Sector Centro-Oriental de la Cuenca del Tajo, Tesis Doctoral. Universidad Complutense de Madrid, 345 pp.

Grimison, N. and Chen, W., 1986, The Azores-Gibraltar Plate Boundary: Focal Mechanisms, Depths of Earthquakes and their Tectonic Implications, *J. Geophys. Res.* **91**, 2029–2047.

Henares Romero, J., López Casado, C. and Delgado J., 2000, Catalogue of focal mechanisms for the Iberian-Maghrebian region. 2^a Asamblea Hispano Portuguesa de Geodesia y Geofísica. Lagos. Portugal.

Henares Romero, J. and López Casado, C., 2001, Catálogo de mecanismos focales del area Ibero-Mogrebí. In: C. López Casado (ed.), *Reprodigital*, Granada. ISBN 84-699-5695-7.

Herraiz, M., De Vicente, G., Lindo Ñaupari, R., Giner, J., Simón, J.L., González Casado, J.M., Vadillo, O., Rodríguez-Pascua, M.A., Cicuéndez, J.I., Casas, A., Cabañas, L., Rincón, P., Cortés, A.L., Ramírez, M. and Lucini, M., 2000, The recent (upper Miocene to Quaternary) and present tectonic stress distributions in the Iberian Peninsula, *Tectonics* **19**, 762–786.

Lisle, R.J., 1987, Principal stress orientations form faults: An additional constraint., *Annales Tectonicae* **1**(2), 155–158.

Lu, Z., Wiss, M., Pulpan, H., 1997, Details of stress directions in the Alaska subduction zone from fault plane solutions, *J. Geophys. Res.* **102**, 5385–5402.

Medina, F. and Cherkaoui, T.E., 1991, Focal mechanisms of the Atlas earthquakes, and tectonic implications., *Geologische Rundschau* **80**/3, 639–648.

Mezcua, J. and Rueda, J., 1997, Seismological evidence for a delamination process in the lithosphere under the Alboran Sea, *Geophys. J. Int.* **129**, 256–264.

Morales, J., Serrano, I., Vidal, F. and Torcal, F., 1997, The depth of the earthquake activity in the Central Betic (Southern Spain), *Geophys. Res. Lett.* **24**, 3289–3292.

Morales, J., Serrano, I., Jabaloy, A., Galindo-Zaldívar, J., Zhao, D., Torcal, F., Vidal, F. and González-Lodeiro, F., 1999, Active continental subduction beneath the Betic Cordillera and the Alborán Sea, *Geology* **27**, 735–738.

Moreira, V.S., 1985, Seismotectonics of Portugal and its adjacent area in the Atlantic, *Tectonophysics* **117**, 85–96.

Pegora, O., 1972, Application de la microtectonique à un étude de neotectonique. Le golfe Maliaque (Grèce centrale, Thèse troisième cycle. U.S.T.L. Montpellier. 41 pp.

Proyecto Sigma, 1998, Análisis del estado de esfuerzos tectónicos, reciente y actual a partir de poblaciones de fallas y mecanismos focales de terremotos. Metodología y aplicación a la Península Ibérica. Colección Otros Documentos, CSN, Madrid.

Sanz de Galdeano, C., 1983, Los accidentes y fracturas principales de las Cordilleras Béticas, *Estudios Geol.* **39**, 157–165.

Sanz de Galdeano, C., 1990, Geologic evolution of the Betic Cordilleras in the Western Mediterranean, Miocene to the present, *Tectonophysics* **172**, 107–119.

Sanz de Galdeano, C., 1996, The E-W segments of the contact between the External and Internal Zones of the Betic and Rif Cordilleras and the E-W corridors of the Internal Zone (A combined explanation), *Estudios Geológicos* **52**, 123–136.

Sanz de Galdeano, C., 1997, La Zona Interna Bético-Rifeña (Antecedentes, unidades tectónicas, correlaciones y bosquejo de reconstrucción paleogeográfica). Monografía Tierras del Sur. Ed. Universidad de Granada, 316 pp.

Seber, D., Barazangi, M., Ibenbrahim, A. and Demnati, A., 1996a, Geophysical evidence for lithospheric delamination beneath the Alboran Sea and Rif-Betic mountains, *Nature* **379**, 785–790.

Seber, D., Barazangi, M., Tadili, B.A., Ramdani, M. and Ben Sari, D., 1996b, Three-dimensional upper mantle structure beneath the intraplate Atlas and interplate Rif mountains of Morocco, *J. Geophys. Res.* **101**, 87, 3125–3138.

Udías, A., 1982, Seismicity and seismotectonic stress field in the Alpine-Mediterranean region, *Geodynamics Series* **7**, 75–82.

Udías, A. and Buforn, E., 1991, Regional Stresses Along the Eurasia-Africa Plate Boundary Derived from Focal Mechanisms of Large Earthquakes, *Pageoph* **136**(4), 433–448.

Udías, A., López Arroyo, A. and Mezcua, J., 1976, Seismotectonic of the Azores-Alboran region., *Tectonophysics* **31**, 259–289.

Van Bemmelem, R.W., 1969, Origin of the Western Mediterraneam Sea, *Geol. Mijnbouw* **26**, 13–52.

Van Bemmelem, R.W., 1972a, Driving forces of Mediterraneam Orogeny (Tyrrhenian Test-case, *Geol. Mijnbouw* **51 (5)**, 548–573.

Van Bemmelem, R.W., 1972b, Geodynamic models (an evaluation and a synthesis). Elsevier, Amsterdam, 267 pp.

Van Bemmelem, R.W., 1973, Geodynamic models for the Alpine type of orogeny (Test-case II: The Alps in Central Europe), *Tectonophysics* **18**, 33–79.

Vissers, R.L.M., Platt, J.P. and Van der Wal, D., 1995, Late orogenic extension of the Betic Cordillera and the Alboran Domain: A lithospheric view, *Tectonics* **14**(4), 786–803.

Wang, K., Mulder, T., Rogers, G.C., Hydman, R.D., 1995, Case for very low coupling stress on the Cascadia subduction pfault, *J. Geophys. Res.* **100**, 12907–12918.